Comparison of different precious metals in activated carbon-supported catalysts for the gas-phase hydrodechlorination of chloromethanes

M. Martin-Martinez*, L.M. Gómez-Sainero, M.A. Alvarez-Montero, J. Bedia, J.J. Rodriguez

Sección Departamental de Ingeniería Química (Departamento de Química-Física Aplicada), Facultad de Ciencias, Universidad Autónoma de Madrid, Cantoblanco, 28049 Madrid, Spain

A B S T R A C T

Four precious metals supported on activated carbon are compared as catalysts in the gas-phase hydrodechlorination (HDC) of chloromethanes. The intrinsic activity or turnover frequency (TOF) of the catalysts follows the order Pd/C > Rh/C > Pt/C > Ru/C in the HDC of dichloromethane (DCM) while the sequence Pd/C > Pt/C > Rh/C > Ru/C was found for the HDC of chloroform (TCM). High selectivities to non-chlorinated products were obtained in all cases except for the HDC of TCM with Rh/C and Ru/C where the selectivity to DCM greatly depends on the operating conditions. A wider diversity of non-chlorinated hydrocarbons was obtained as reaction products with these two catalysts, especially in the HDC of TCM, favoring the formation of carbonaceous deposits which provoked a marked deactivation of the catalysts. In contrast, CH_4 was the only non-chlorinated product obtained with the Pt/C catalysts which showed by far the highest stability. Different reaction pathways were found depending on the catalyst and the starting chloromethane. The different reactivity of the metals is explained in terms of their different electronic structure and the physicochemical properties of the catalysts.

© 2012 Elsevier B.V. All rights reserved.

1. Introduction

Chloromethanes (CM) are chlorinated volatile organic compounds with high toxicity and carcinogenic character. They contribute to global warming, the depletion of the ozone layer and the formation of photochemical smog [1–3]. Despite their harmful effects and because of their particular physical and chemical properties (high stability, low flammability, high volatility, high solvent capacity), these compounds are still widely used in the chemical and pharmaceutical industry as solvents, dry-cleaners, degreasing agents, adhesive components, etc. Consequently, large amounts of these pollutants are still released into the environment through liquid and gas streams. Their emissions have been progressively restricted by stringent legal regulations, so that the development of suitable technologies for the treatment of industrial effluents contaminated by these compounds is necessary. Catalytic hydrodechlorination (HDC) has a great potential in that respect since it can operate under ambient pressure and relative low temperature, the selectivity to reaction products can be modified using different catalysts and it is applicable over a wide range of pollutant concentrations [4–6].

In recent years, a growing number of studies related to the HDC of different chlorocarbons and chlorofluorocarbons with catalysts based on different metals and supports has been published. Precious metals, such as palladium, platinum, rhodium and ruthenium have been tested as active phases. Among them, palladium and platinum are very well considered, the first because of its high activity and selectivity to non-chlorinated products [7–9] and the second because of its superior stability [10–15]. Other studies indicated that other catalysts, like Ru/C and Ru/SiO_2, were more stable than Pd, Pt or Rh supported on activated carbon or silica in the HDC of CFC-113 [16]. Gómez-Sainero et al. [17] used Pd, Pt, Rh and Ru supported on activated carbon as catalysts for the HDC of tetrachloromethane (TTCM), finding that the activity followed the order Pd/C ≫ Pt/C > Rh/C > Ru/C. Benitez et al. [18] studied the HDC of different aromatic chlorinated compounds with three activated carbon-supported catalysts, finding that the activity followed the order Pd/C ≫ Ru/C > Rh/C. As mentioned above, the selectivity to reaction products also changes depending on the catalyst. Kovalchuk and d'Itri [19] studied the HDC of different chlorocarbons and chlorofluorocarbons with group VIII metal catalysts and found that, with Pd and Pt, saturated hydrocarbons were formed whereas, when other metals were added, higher selectivities to unsaturated hydrocarbons were observed.

The number of publications related to the use of activated carbons in catalysis has noticeably grown, because of their interesting physical and chemical properties as well as their price, which is lower than for other support materials [20,21]. Amorim et al.

* Corresponding author at: Ingeniería Química, Facultad de Ciencias, Universidad Autónoma de Madrid, Campus de Cantoblanco, Ctra. Colmenar Km 15, 28049 Madrid, Spain. Tel.: +34 91 497 5599; fax: +34 91 497 3516.
E-mail address: maria.martin.martinez@uam.es (M. Martin-Martinez).

[22] studied the feasibility of using activated carbon, graphite and graphitic carbon nanofibers as supports for palladium catalysts in chlorobenzene HDC finding the lowest activity with graphite. Legawiec-Jarzyna et al. [13] tested three platinum catalysts supported on alumina, activated carbon and silica in the HDC of TTCM, finding the lowest selectivity to chloroform (TCM) with Pt/C.

So far there is a scarce literature dealing with the HDC of CMs other than TTCM. Some studies using palladium and platinum [9,14,15,23–25] and a few with rhodium and ruthenium catalysts [9,26] have been published. However, to the best of our knowledge, there is a lack of comparative studies on the performance of precious metals in the HDC of TCM, dichloromethane (DCM) and monochloromethane (MCM).

In a previous work [9] a preliminary study comparing the HDC of DCM with four different activated carbon-supported catalysts (Pd/C, Pt/C, Rh/C, Ru/C) was presented. All the catalysts tested were shown to be fairly active although there were significant differences, not only in activity, but in selectivity and stability also. The HDC of MCM, DCM and TCM with Pd/C and Pt/C was investigated in previous work [14,15,24]. Both catalysts were highly selective to non-chlorinated products although with significant differences in product distribution. However, while Pd/C showed a higher activity, Pt/C was by far more stable. The aim of this work is to analyze in depth the different behavior of four metallic phases (Pd, Pt, Rh and Ru) supported on activated carbon as catalysts in the gas-phase HDC of MCM, DCM and TCM and establish the reaction pathways.

2. Experimental

2.1. Catalysts preparation

Four monometallic catalysts of Pd, Pt, Rh and Ru supported on a commercial activated carbon (whose characteristics have been reported elsewhere [27]) were prepared by incipient wetness impregnation, using aqueous solutions of $PdCl_2$, H_2PtCl_6, $RhCl_3$ and $RuCl_3$ (supplied by *Sigma–Aldrich*) of the required concentrations to obtain 1 wt% active phase nominal loading. The catalysts were dried overnight at room temperature and heated to 100 °C at 20 °C h^{-1}, the final temperature being maintained for 2 h. The activation of all the catalysts was carried out by heating them up to 250 °C (at 10 °C min^{-1}) under a continuous H$_2$ flow (50 N cm^3 min^{-1}, supplied by *Praxair* with a minimum purity of 99.999%) and maintaining these conditions for 2 h.

2.2. Catalysts characterization

N$_2$ adsorption–desorption isotherms (77 K) were obtained to characterize the porous structure of the catalysts (*TriStar II 3020, Micromeritics*). The samples were previously outgassed for 12 h at 150 °C (*VacPrep 061, Micromeritics*). The surface area was calculated by the BET equation and the *t*-method was used to obtain micropore volume.

Bulk metal content was determined via inductively coupled plasma-mass spectrometry (*ICP-MS Elan 6000, PerkinElmer Sciex*). The samples were previously digested in a strongly acidic mixture and then treated in a microwave oven (*Milestone ETHOS PLUS*).

Metal dispersion on the catalysts surface was determined by CO chemisorption at room temperature (*PulseChemiSorb 2705, Micromeritics*). The samples were previously reduced under a continuous H$_2$ flow of 50 N cm^3 min^{-1} at 250 °C for 2 h and then cooled to room temperature under a He flow of 30 N cm^3 min^{-1}. The metal dispersion was calculated from the CO chemisorption data. The stoichiometry of the CO adsorption on the metal atoms was assumed to be 1 [28–32].

The surface composition of the catalysts was analyzed by X-ray photoelectron spectroscopy (XPS) (*5700C Multitechnique System, Physical Electronics*), using Mg Kα (1253.6 eV) radiation. The elements present at the surface of the catalysts were determined by recording general XPS spectra, scanning up to a binding energy (BE) of 1200 eV. Corrections for changes in BE caused by sample charging was effected by taking the C1s peak (284.6 eV) as an internal standard. The BE of the Pd 3d$_{5/2}$, Pt 4f$_{7/2}$, Rh 3d$_{5/2}$ and Ru 3d$_{5/2}$ core levels and full width at half maximum (FWHM) values were used to assess the chemical state of these metals at the catalyst surface.

2.3. Catalytic activity experiments

The HDC experiments were conducted in a continuous flow reaction system described elsewhere [24], consisting of a quartz fixed bed micro-reactor coupled to a gas-chromatograph with an FID detector to analyze the reaction products.

The working conditions used were: atmospheric pressure, a total gas flow rate of 100 N cm^3 min^{-1}, a CM inlet concentration of 1000 ppmv and a H$_2$/CM molar ratio of 100. The catalyst mass and reaction temperature were adjusted to the desired values in each run. Space–times (τ) in the range of 0.04–1.73 kg h mol^{-1} and reaction temperatures of 150–250 °C were used. Long term experiments were performed at a space time of 1.73 kg h mol^{-1} and a reaction temperature of 250 °C.

The behavior of the catalysts was evaluated in terms of CM conversion, turnover frequency (*TOF*), selectivity to the different reaction products and yield values. The evolution of the catalytic activity as a function of time on stream was also studied.

3. Results and discussion

3.1. Characterization of the catalysts

Table 1 summarizes the values of BET surface area, micropore volume, bulk metal content and metal dispersion of the fresh and used (100 h on stream) catalysts.

The 77 K N$_2$ adsorption–desorption isotherms of the catalysts (not shown) approached Type 1 of the DBBT classification [33] indicating that they were essentially microporous solids, although they presented hysteresis Type H-4 (IUPAC) cycles due to the contribution of mesopores. All the fresh catalysts had a high BET surface area, around 1100 m^2 g^{-1}, which remained basically unaltered during use except in the cases of Rh/C and Ru/C in the HDC of TCM where a substantial reduction in SSA was observed. This could be related to the blockage of the porous structure by carbonaceous deposits as will be explained below.

The results of CO chemisorption indicated that the metal phase was fairly well dispersed in all the fresh catalysts. In agreement with the results obtained in previous work [9,14,15], a significant decrease of the metal dispersion was observed for Pd/C, Rh/C and Ru/C after their use in HDC whereas the dispersion of the Pt/C catalyst actually increased in the HDC of DCM and of TCM. Re-dispersion of metallic particles for Pt/C catalysts after its use in the HDC of DCM was evidenced by TEM [15]. It was ascribed to the presence of HCl that involves the formation, volatilization and re-deposition of unstable metallic chlorides. These chlorides can be reduced by the high concentration of H$_2$ introduced as reactant. In the HDC of DCM, the decrease in dispersion was more pronounced in the case of Ru/C. In a previous study [9] metal sintering was observed in Ru/C used in the HDC of DCM while no significant changes of metal particle size were observed in the Pd/C, Pt/C and Rh/C catalysts under the same conditions. The decrease in metal dispersion then observed for Pd/C and Rh/C was attributed to the poisoning of active centers with reactants, intermediates and/or reaction

Table 1
Metal content, porous structure and dispersion of the fresh and used catalysts.

Catalyst	Metal content (%)	S_{BET} (m^2 g^{-1})	Micropore volume (cm^3 g^{-1})	Dispersion (%)
Pd/C	0.86	1100	0.52	26
Pd/C used MCM	0.95	1113	0.52	20
Pd/C used DCM	0.85	1141	0.54	11
Pd/C used TCM	0.93	1192	0.54	12
Pt/C	0.85	1136	0.53	24
Pt/C used MCM	0.84	1193	0.55	22
Pt/C used DCM	0.83	1123	0.52	32
Pt/C used TCM	0.83	1167	0.53	34
Rh/C	0.80	1110	0.53	32
Rh/C used MCM	0.78	1123	0.51	25
Rh/C used DCM	0.80	1098	0.52	21
Rh/C used TCM	0.82	260	0.12	2
Ru/C	0.88	1116	0.53	20
Ru/C used MCM	0.81	1111	0.51	11
Ru/C used DCM	0.81	941	0.44	2
Ru/C used TCM	0.83	404	0.18	3

products. In the current contribution, the remarkable decrease in the dispersion of Ru/C and Rh/C when used in the HDC of TCM can be attributed to the blockage of the porous structure as stated above.

Table 2 summarizes the results of XPS analysis for each catalyst when fresh, reduced and after 100 h on stream. In the case of Ru/C, the XPS data were not used because of the low intensity of the spectra. This means that Ru particles may have been mainly deposited in the internal pores instead of on the outermost surface of the catalyst. As in previous work, the existence of two different species, zero-valent (M^0) and electrodeficient (M^{n+}) metals were observed, with a higher proportion of the former in Pt/C than in Pd/C and Rh/C. The latter two catalysts showed similar performance and the proportion of M^{n+} species decreased after their use in HDC. On the contrary, no significant changes were found in the proportion of the different Pt species in the Pt/C catalyst upon use. This behavior has been related to the different contribution of zero-valent and electrodeficient species as active centers for the dissociative adsorption of CM in the different catalysts [14,24,27]. There were also several differences in the distribution of the metal phase on the support. Rh/C presented a high metallic concentration on the outer surface while Pd and Pt particles seemed to be more homogeneously distributed throughout the porous structure of the catalyst, especially in the case of Pt/C where the bulk concentration of Pt was very similar to that measured by XPS. As shown in Table 2, a remarkable increase in the amount of organic chloride is observed for Rh/C catalyst after used in the HDC of TCM, which can be attributed to the formation of chlorinated carbonaceous deposits in accordance with the results obtained by N_2 adsorption and CO chemisorption. In the HDC of DCM, the amount of organic chloride is somewhat higher for Pd/C and Rh/C, while no increase is observed for Pt/C, in accordance with the results previously reported [15].

3.2. Catalytic activity

Figs. 1–3 show the evolution of MCM, DCM and TCM conversion, respectively, with space–time, at different temperatures for all the catalysts tested. As can be seen, HDC proceeded with all the catalysts at a significantly lower rate in the case of MCM confirming that the trend in the reactivity of CMs is for it to increase with increasing chlorine content of the molecule [14,34]. The Pd catalyst was by far the most active in the MCM HDC and also showed the highest activity with TCM, in this case very similar to that of Pt. In the case of DCM, the Pd catalyst conversion was somewhat below Rh, where this metal was the most active. Complete conversion of TCM was achieved with all the catalysts although Rh/C and Ru/C required significantly higher space–time.

Table 3 collects the initial reaction rate and TOF values for HDC of DCM and TCM for all the catalysts tested at different temperatures. The initial reaction rates were calculated from the experiments performed at low space–time values (reported as supplementary data), where conversion and space–time follow a linear relationship. The results of Table 3 serve to refine the previous conclusions from Figs. 2 and 3, and include the values of apparent activation energy.

In the HDC of DCM, the activity of the catalysts followed the order Pd/C > Rh/C > Pt/C > Ru/C while in the HDC of TCM the sequence is Pd/C > Pt/C > Rh/C > Ru/C. These trends can be related to the electronic properties of the metals. The local density of unoccupied states at the Fermi level ($N(E_f)$) can be used to characterize the intrinsic electronic structure of each metal. It measures the number of quantum states available for bonding reactants [35] and it has been used by various authors to explain the catalytic activity of group VIII metals [17,36–39]. As $N(E_f)$ values are not easily available, a property such as the magnetic susceptibility (χ), which directly depends on it, can be used [35–40]. The χ values for these metals follow the sequence Pd > Pt > Rh > Ru [17,41]. It is assumed that the CM molecule is heterolytically dissociated and adsorbed through the terminal electron-donating chlorine, thus the higher the density of unoccupied states of the metal, the higher the reactivity with the electron–donor species and a higher activity of the catalyst can be expected [17,42]. The above sequence of density of unoccupied states is consistent with that found for the catalytic activity in the HDC of TCM in this study. The same sequence has been reported in the literature for liquid-phase HDC of TTCM [17]. In the case of DCM the lower activity of Pt/C compared to Rh/C can be attributed to the lower proportion of electro-deficient species (Pt^{n+}) in the former (Table 2). Though $N(E_f)$ is an intrinsic property of metals, its value can be modified by different factors, such as the oxidation state of metal, crystal geometry and chemical environment. By considering the values of the dissociation energy for the chlorine–carbon bond (325 kJ mol^{-1} for TCM and 339 kJ mol^{-1} for DCM) [43], it is seen that the dissociation of TCM is favored, so that the effect of electro-deficient species is not as important as in the HDC of DCM.

Substantial differences were also found in the selectivity to the reaction products. CH_4 is the only reaction product in the HDC of MCM with all the catalysts, while with the two other CM hydrocarbons, products containing up to four carbon atoms were obtained, depending on the catalyst. Figs. 4 and 5 show the evolution of the selectivity of the catalysts with space–time in the HDC of DCM and TCM, respectively, at a reaction temperature of 250 °C. MCM is the only chlorinated byproduct in the HDC of DCM and all the catalysts were highly selective to non-chlorinated products with

Table 2
Surface composition of the fresh, reduced and used (100 h on stream) catalysts.

Catalyst	M_{XPS} (%)	M^0 (%)	M^{n+} (%)	M_{XPS}/M_{BULK}	Cl_{XPS} (%)	$Cl_{inorg.}$ (%)	$Cl_{org.}$ (%)
Pd/C	0.17	4.5	95.5	1.75	0.35	49.2	50.8
Pd/C reduced	0.32	52.9	47.1	3.30	0.11	46.7	53.3
Pd/C used MCM	1.35	59.1	40.9	12.59	0.25	65.4	34.6
Pd/C used DCM	0.25	62.3	37.7	2.61	0.13	29.2	70.8
Pd/C used TCM	0.95	65.7	34.3	9.05	1.36	16.0	84.0
Pt/C	0.06	52.1	47.9	1.15	0.43	37.6	62.4
Pt/C reduced	0.07	74.5	25.5	1.34	0.13	17.0	83.0
Pt/C used MCM	0.03	78.6	21.4	0.58	0.11	30.2	69.8
Pt/C used DCM	0.04	68.9	31.1	0.78	0.14	18.5	81.5
Pt/C used TCM	0.05	76.2	23.8	0.98	1.44	8.5	91.5
Rh/C	2.08	12.6	87.4	22.28	0.85	57.7	42.3
Rh/C reduced	1.72	35.9	64.1	18.42	0.38	54.9	45.1
Rh/C used MCM	2.46	34.8	65.2	27.02	0.59	27.9	72.1
Rh/C used DCM	2.19	44.8	55.2	23.45	0.51	48.5	51.5
Rh/C used TCM	1.80	75.1	24.9	18.81	5.38	4.7	95.3

M: metal (Pd, Pt or Rh).

selectivities well above 80%, and approaching 95% in the case of Pd/C and Rh/C (Fig. 4). No significant changes of selectivity were found within the range of space–time studied, with the exception of the appearance of alkenes at low space–times with Ru/C catalysts which were further transformed to the corresponding alkanes. This also occurred with the Pd/C and Pt/C catalysts in the HDC of TCM, where very low selectivity to chlorinated products was observed across the whole range of space–time explored (Fig. 5). Fairly high selectivities to non-chlorinated products were obtained for both catalysts, but especially with Pd/C which yielded values above 95% even at the lowest space–time tested. In contrast, very high selectivities to DCM were found with Rh/C and Ru/C at low space–times, especially for the latter, where 100% selectivity to DCM was obtained at the lowest space–time. In addition, higher selectivities to alkenes were observed for these two catalysts, indicating that Rh and Ru had lower hydrogenation capacities. When increasing the space–time, a significant decrease in the selectivity of DCM was observed, in favor of non-chlorinated

hydrocarbons, which suggests that DCM is an intermediate product. Nevertheless, in the case of Ru catalysts, DCM selectivity remains very high (near 30%) even at the highest space–time investigated.

When increasing the reaction temperature, a significant decrease of the selectivity to MCM was observed in the HDC of DCM, except with the Ru catalyst, which showed the opposite behavior (Fig. 6). This can be related to the stronger tendency of this metal to sinter, which would become more significant as the temperature increased, hindering the supply of hydrogen to the active centers. The presence of small metal particles has been found to be crucial for providing high concentrations of H_2 in the vicinity of the CM adsorption centers [15,44]. In the HDC of TCM a slight increase of the selectivity to MCM with temperature was observed with Ru/C and Rh/C while no significant effect was observed with Pd/C and Pt/C (Fig. 7). The selectivity to DCM strongly decreases with increasing reaction temperature for all the catalysts at high space–time.
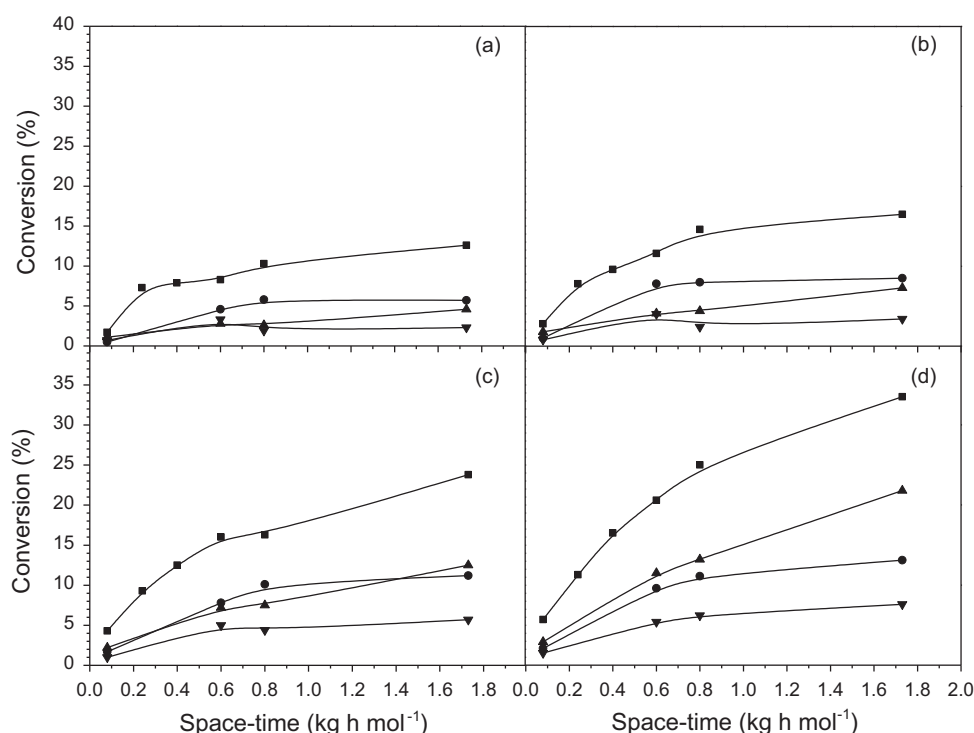
Fig. 1. Conversion vs. space–time in the HDC of MCM at 175 °C (a), 200 °C (b), 225 °C (c) and 250 °C (d) with the different catalysts: Pd/C (■), Pt/C (●), Rh/C (▲) and Ru/C (▼).
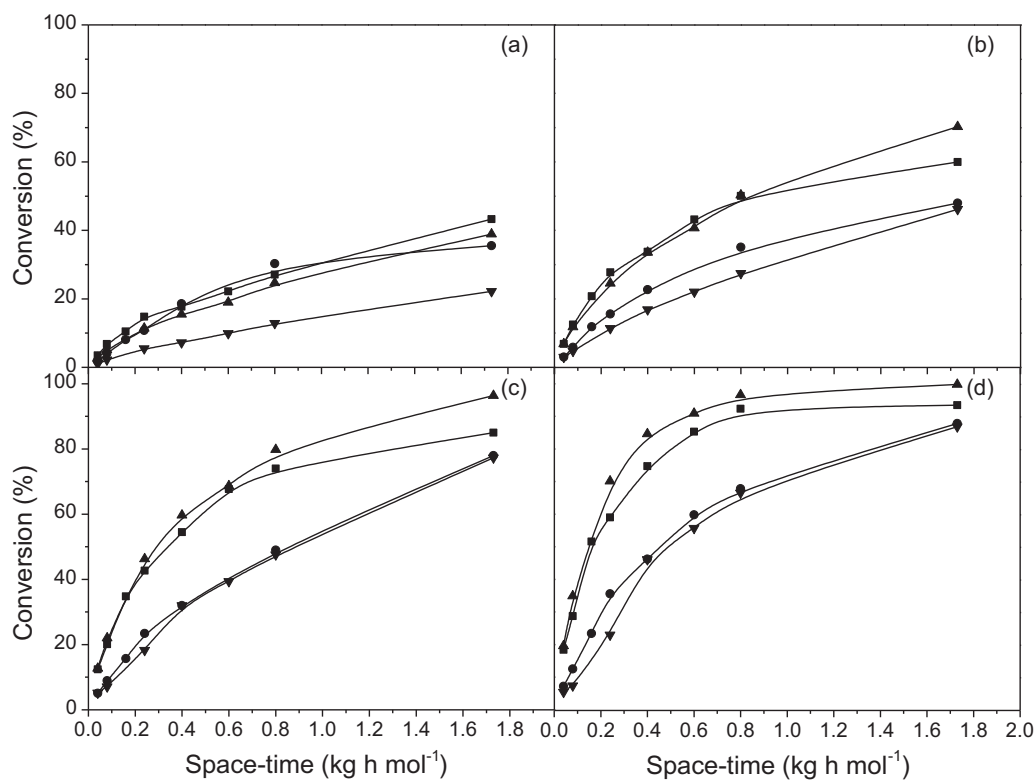
Fig. 2. Conversion vs. space–time in the HDC of DCM at 175 °C (a), 200 °C (b), 225 °C (c) and 250 °C (d) with the different catalysts: Pd/C (■), Pt/C (●), Rh/C (▲) and Ru/C (▼).

As reported in a recent work [15], methane was the only non-chlorinated product from HDC of DCM and TCM with the Pt/C catalyst. The three other catalysts yielded increasingly diverse product distributions following the order Ru/C > Rh/C > Pd/C and

TCM > DCM. In the HDC of DCM, methane was by far the main product with all the catalysts, followed by ethane. Small amounts of propane were obtained with Pd/C and significantly larger amounts with Rh/C and Ru/C. With Ru/C, small amounts of ethene and
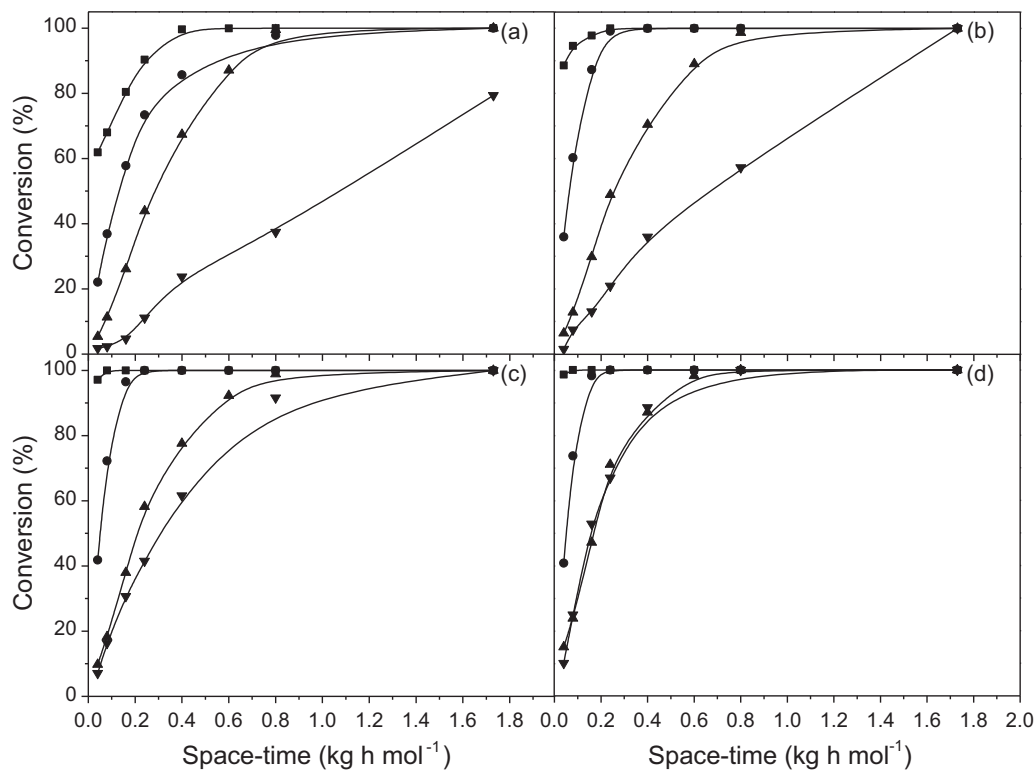

Fig. 3. Conversion vs. space–time in the HDC of TCM at 175 °C (a), 200 °C (b), 225 °C (c) and 250 °C (d) with the different catalysts: Pd/C (■), Pt/C (●), Rh/C (▲) and Ru/C (▼).

Table 3
Initial rate (r_{CM}), initial TOF and apparent activation energy (E_a) for the HDC of DCM and TCM with the catalysts tested.

Catalyst	T (°C)	HDC of DCM			HDC of TCM		
		$r_{CM} \times 10^2$ (mol g_M^{-1} h^{-1})	E_a (kJ mol^{-1})	TOF (h^{-1})	$r_{CM} \times 10^2$ (mol g_M^{-1} h^{-1})	E_a (kJ mol^{-1})	TOF (h^{-1})
Pd/C	125				23.95		98.02
	150	3.33		13.64	105.23		430.72
	175	9.88		40.45	179.94		736.52
	200	18.10	50.9	74.07	257.56	32.4	1054.21
	225	36.00		147.33	282.27		1155.34
	250	53.94		220.79	286.63		1173.19
Pt/C	150	1.18		9.56	20.20		164.20
	175	3.06		24.86	41.18		334.70
	200	5.29	52.5	43.03	88.68	32.4	720.81
	225	11.55		93.88	106.18		863.06
	250	21.32		173.33	108.24		879.79
Rh/C	150				14.69		47.23
	175	7.84		25.22	17.66		56.78
	200	18.17	50.3	58.44	20.16	17.1	64.82
	225	33.84		108.82	30.23		97.21
	250	54.30		174.61	36.24		116.55
Ru/C	150	0.98		4.94			
	175	2.55		12.89	4.94		24.99
	200	5.17	44.4	26.14	10.09	41.4	50.97
	225	8.27		41.78	19.95		100.83
	250	10.66		53.89	33.12		167.35

M: metal (Pd, Pt, Rh or Ru).

propene were also detected. In the HDC of TCM the selectivity to methane is markedly lower in all cases in favor of larger hydrocarbons. Ethane was the main product with Pd/C, propane was obtained in somewhat lower percentage than methane and small amounts of ethene and propene were produced. With Rh/C and Ru/C butane and butene were also formed and the selectivity to alkenes was higher with these two catalysts. According with these findings, our previous results [9,14,15] and the

information reported in Tables 1 and 2 concerning the characterization of the fresh and used catalysts, the formation of hydrocarbons of more than one carbon atom appears to be favored by the following factors: (I) A higher ratio of electro-deficient to zero-valent metallic species, since Pt/C – which yielded methane as the only non-chlorinated byproduct – presented most of the metal in the zero-valent state while Pd/C and Rh/C show higher proportions of electro-deficient species. (II) A lower dispersion of the active phase.
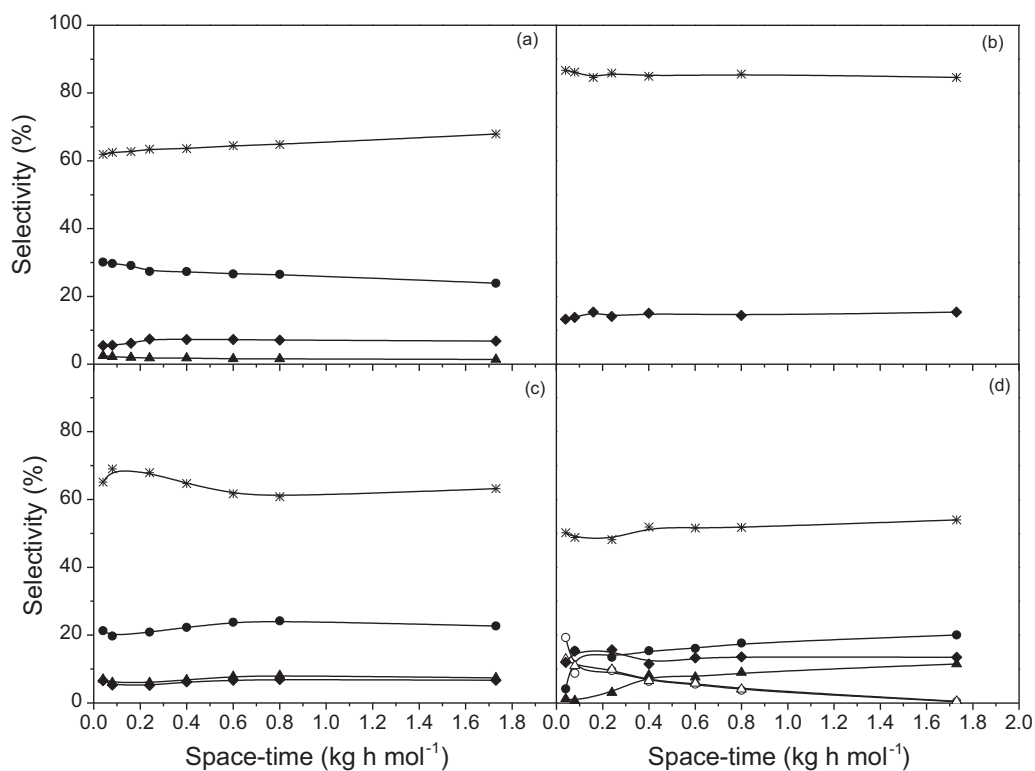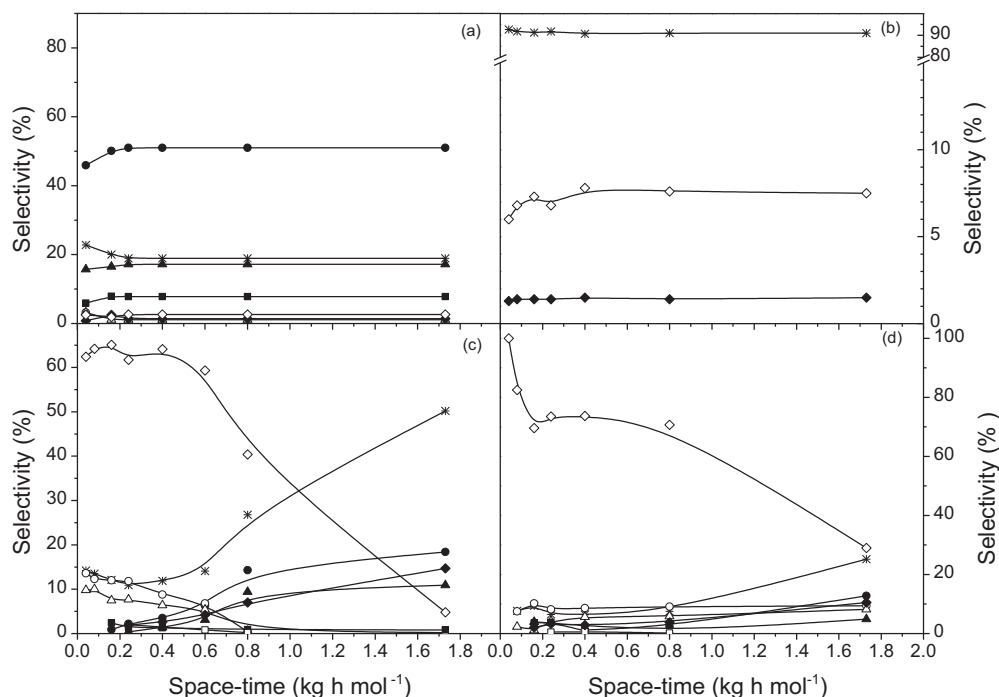

Fig. 4. Evolution of the selectivity to reaction products with space–time in the HDC of DCM with Pd/C (a), Pt/C (b), Rh/C (c) and Ru/C (d) at 250 °C: CH$_4$ (*); C$_2$H$_6$ (●); C$_2$H$_4$ (○); C$_3$H$_8$ (▲); C$_3$H$_6$ (△); MCM (♦).

Fig. 5. Evolution of the selectivity to reaction products with space–time in the HDC of TCM with Pd/C (a), Pt/C (b), Rh/C (c) and Ru/C (d) at 250 °C: CH_4 (*); C_2H_6 (●); C_2H_4 (○); C_3H_8 (▲); C_3H_6 (△); C_4H_{10} (■); C_4H_8 (□); MCM (♦); DCM (◇).

Dispersion did not diminish and even increased during time on stream in the case of Pt/C whereas a decrease was observed for the rest of the catalysts, most especially in the case of Ru/C, the catalyst yielding the widest product distribution [9]. (III) A less homogeneous distribution of the active species on the catalyst: The ration

of XPS to bulk metal concentration is much higher for Rh/C than for Pt/C or Pd/C (see Table 2) indicating that Rh is mainly deposited on the outermost surface of the activated carbon whereas Pd and especially Pt are more homogeneously distributed throughout the porous structure of the support. As indicated before, Ru appears
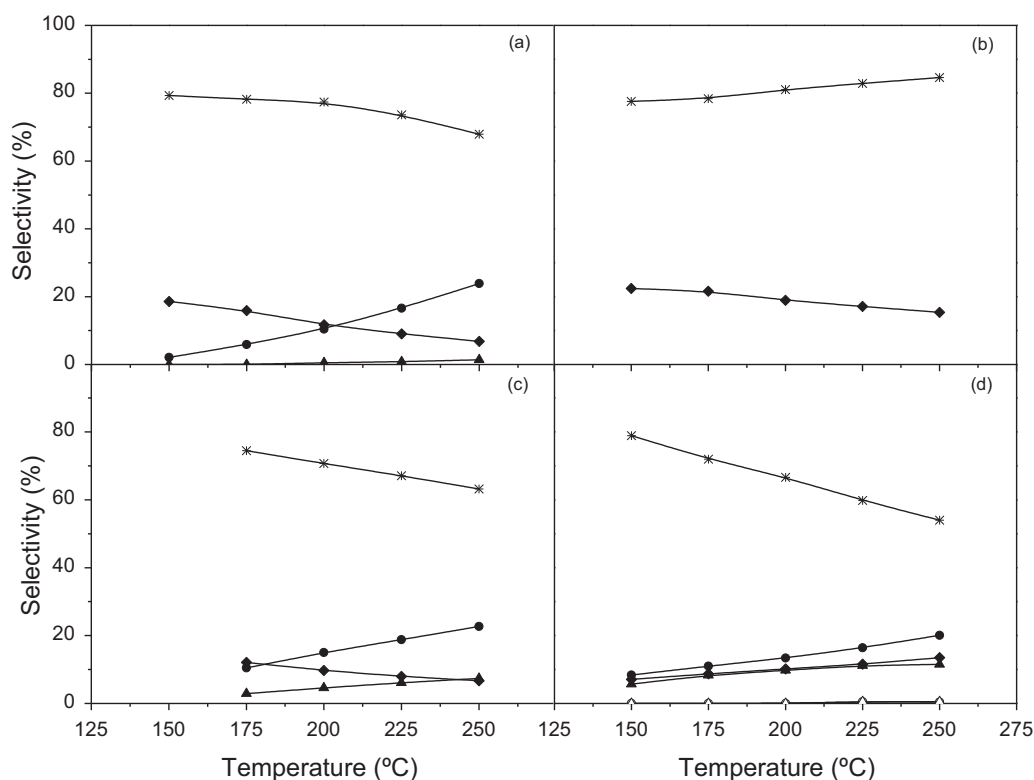

Fig. 6. Evolution of the selectivity to reaction products with temperature in the HDC of DCM with Pd/C (a), Pt/C (b), Rh/C (c) and Ru/C (d) at 1.73 kg h mol^{-1}: CH_4 (*); C_2H_6 (●); C_2H_4 (○); C_3H_8 (▲); C_3H_6 (△); MCM (♦).
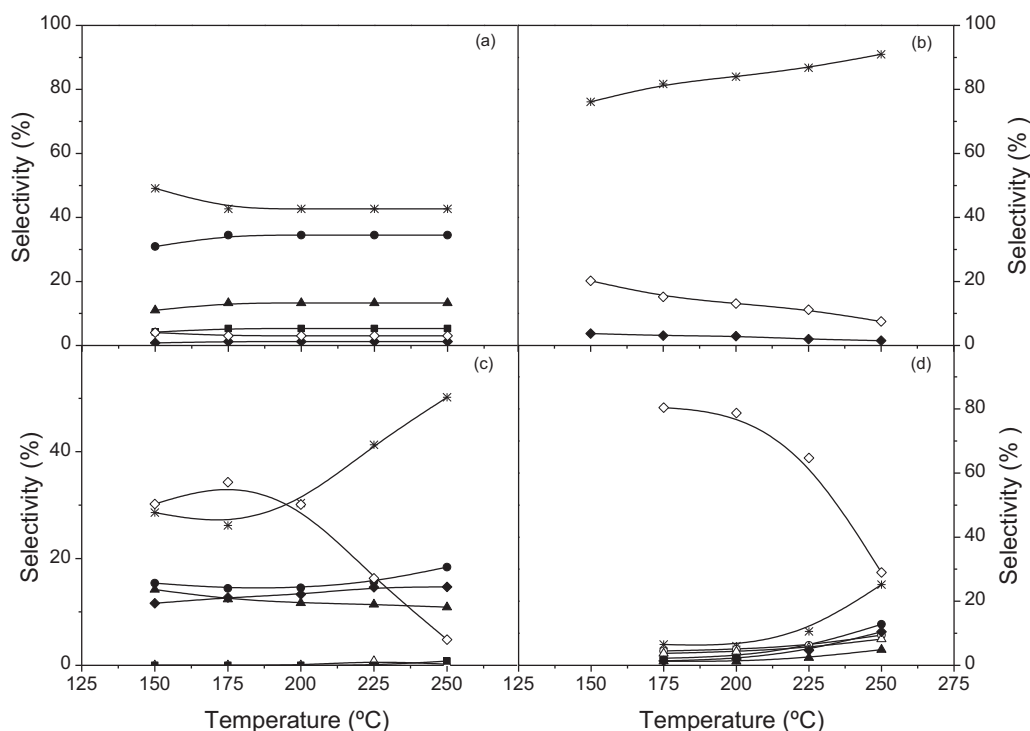
Fig. 7. Evolution of the selectivity to reaction products with temperature in the HDC of TCM with Pd/C (a), Pt/C (b), Rh/C (c) and Ru/C (d) at 1.73 kg h mol^{-1}: CH$_4$ (*); C$_2$H$_6$ (●); C$_2$H$_4$ (○); C$_3$H$_8$ (▲); C$_3$H$_6$ (△); C$_4$H$_{10}$ (■); MCM (♦); DCM (◊).

to be mainly deposited inside the pores and it is very prone to sintering.
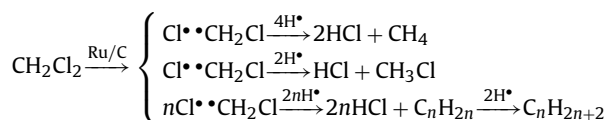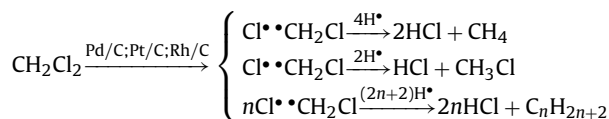
With regard to the stability of the catalysts, important differences were found over the long term experiments described here. In the HDC of DCM the stability followed the order Pt/C > Rh/C > Pd/C > Ru/C. After 100 h on stream, the Pt/C catalyst did not show any deactivation, while a loss of activity of 19%, 31% and 82% was found for Rh/C, Pd/C and Ru/C, respectively. In the HDC of TCM, the greatest deactivation was found for Ru/C and Rh/C with a loss of activity of 75% after 58 and 95 h on stream, respectively. This can be ascribed to the formation of carbonaceous deposits as the BET surface area of the catalysts greatly decreases after their use in the HDC reaction (Table 1). This is consistent with the lower hydrogenation activity of these catalysts which led to larger amounts of long-chain hydrocarbons.

3.3. Reaction scheme

From the evolution of product distribution with space–time (Figs. 8 and 9) the corresponding reaction schemes are proposed. In the HDC of DCM, except with the Ru/C catalyst, all the species showed a finite rate of formation approaching zero space–time, indicating that all of them are primary products formed from the DCM-derived chloride radical (Fig. 8). The same evidence was suggested by the evolution of the products selectivities (Fig. 4). These show positive intercepts when extrapolating to zero space–time. Nevertheless, with the Ru/C catalyst it can be seen that ethane and propane appear as ethylene and propylene disappear, indicating that these saturated hydrocarbons are secondary products formed from their unsaturated homologues (Fig. 4).
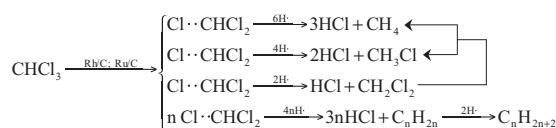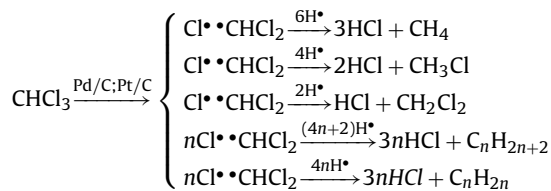
As stated in previous studies [14,24,27,45,46] the HDC reaction proceeds through the dissociative adsorption of both CM and H$_2$ on the catalyst surface and the formation of hydrocarbons larger than methane is due to the reaction between two organochlorinated

radicals adsorbed on two neighboring centers [14,24,27]. Thus, the following reaction schemes can be proposed for the HDC of DCM, depending on the catalyst used:

$$CH_2Cl_2 \xrightarrow{Pd/C;Pt/C;Rh/C} \begin{cases} Cl\bullet \bullet CH_2Cl \xrightarrow{4H^\bullet} 2HCl + CH_4 \\ Cl\bullet \bullet CH_2Cl \xrightarrow{2H^\bullet} HCl + CH_3Cl \\ nCl\bullet \bullet CH_2Cl \xrightarrow{(2n+2)H^\bullet} 2nHCl + C_nH_{2n+2} \end{cases}$$

$$CH_2Cl_2 \xrightarrow{Ru/C} \begin{cases} Cl\bullet \bullet CH_2Cl \xrightarrow{4H^\bullet} 2HCl + CH_4 \\ Cl\bullet \bullet CH_2Cl \xrightarrow{2H^\bullet} HCl + CH_3Cl \\ nCl\bullet \bullet CH_2Cl \xrightarrow{2nH^\bullet} 2nHCl + C_nH_{2n} \xrightarrow{2H^\bullet} C_nH_{2n+2} \end{cases}$$

With regard to TCM (Figs. 5 and 9), all the reaction products with the Pd/C and Pt/C catalysts appear to be primary while with Rh/C and Ru/C it can be appreciated that whereas the evolution of MCM, methane, ethane and propane versus space–time follow a continuously increasing trend, that of ethylene and propylene show maxima.

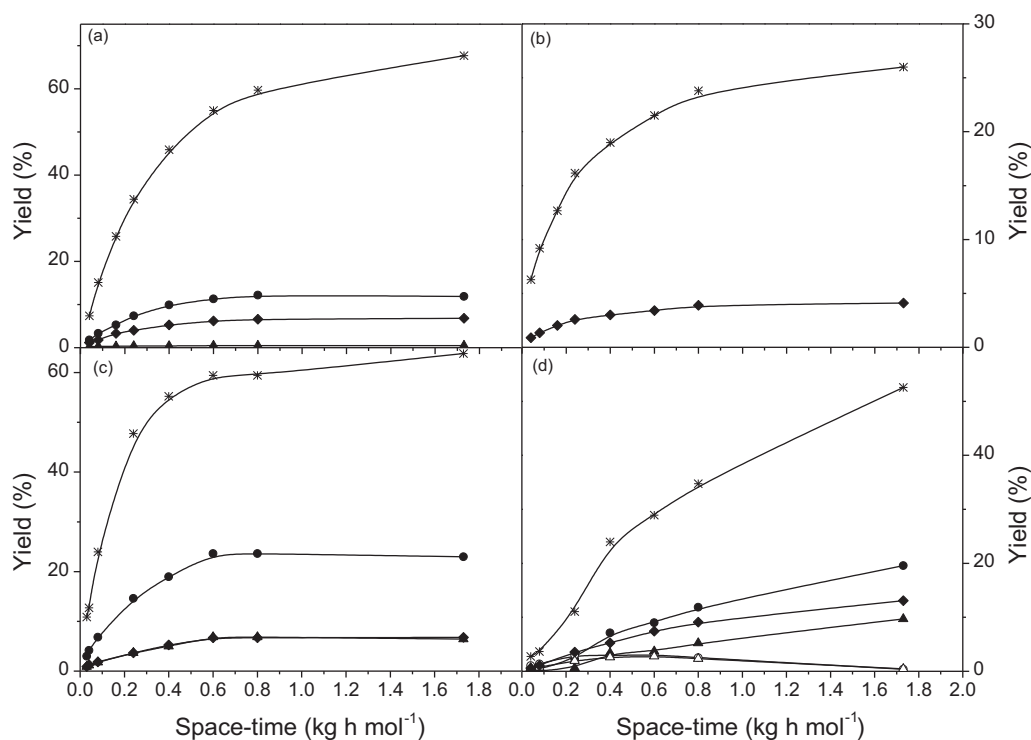Thus, the following reaction schemes are proposed for the HDC of TCM:

$$CHCl_3 \xrightarrow{Pd/C;Pt/C} \begin{cases} Cl\bullet \bullet CHCl_2 \xrightarrow{6H^\bullet} 3HCl + CH_4 \\ Cl\bullet \bullet CHCl_2 \xrightarrow{4H^\bullet} 2HCl + CH_3Cl \\ Cl\bullet \bullet CHCl_2 \xrightarrow{2H^\bullet} HCl + CH_2Cl_2 \\ nCl\bullet \bullet CHCl_2 \xrightarrow{(4n+2)H^\bullet} 3nHCl + C_nH_{2n+2} \\ nCl\bullet \bullet CHCl_2 \xrightarrow{4nH^\bullet} 3nHCl + C_nH_{2n} \end{cases}$$

$$CHCl_3 \xrightarrow{Rh/C; Ru/C} \begin{cases} Cl\cdot\cdot CHCl_2 \xrightarrow{6H\cdot} 3HCl + CH_4 \leftarrow \\ Cl\cdot\cdot CHCl_2 \xrightarrow{4H\cdot} 2HCl + CH_3Cl \leftarrow \\ Cl\cdot\cdot CHCl_2 \xrightarrow{2H\cdot} HCl + CH_2Cl_2 \\ n\,Cl\cdot\cdot CHCl_2 \xrightarrow{4nH\cdot} 3nHCl + C_nH_{2n} \xrightarrow{2H\cdot} C_nH_{2n+2} \end{cases}$$

Fig. 8. Evolution of the yield to reaction products with space–time in the HDC of DCM with Pd/C (a), Pt/C (b), Rh/C (c) and Ru/C (d) at 250 °C: CH$_4$ (*); C$_2$H$_6$ (●); C$_2$H$_4$ (○); C$_3$H$_8$ (▲); C$_3$H$_6$ (△); MCM (♦).
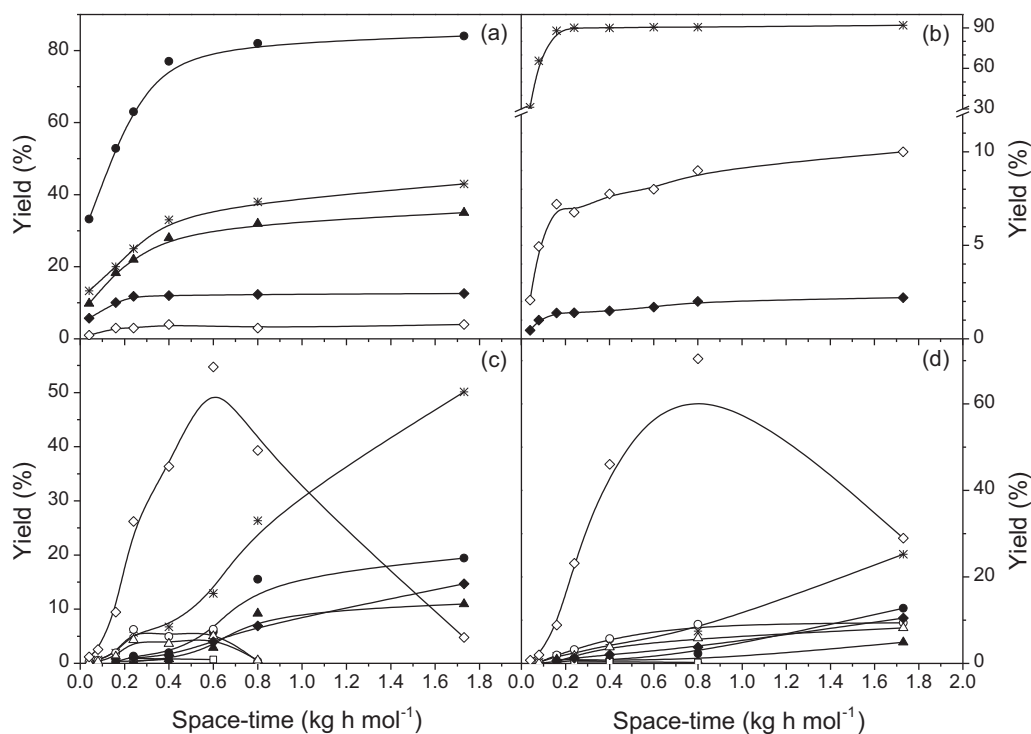

Fig. 9. Evolution of the yield to reaction products with space–time in the HDC of TCM with Pd/C (a) at 175 °C, and Pt/C (b), Rh/C (c) and Ru/C (d) at 250 °C: CH$_4$ (*); C$_2$H$_6$ (●); C$_2$H$_4$ (○); C$_3$H$_8$ (▲); C$_3$H$_6$ (△); C$_4$H$_{10}$ (■); C$_4$H$_8$ (□); MCM (♦); DCM (◇).

4. Conclusions

The activated carbon-supported catalysts prepared using Pd, Pt, Rh and Ru as active phases have been demonstrated to be effective in the gas phase HDC of MCM, DCM and TCM, the reactivity following the order TCM > DCM > MCM. In the HDC of DCM, the activity of the catalysts follows the order Pd/C > Rh/C > Pt/C > Ru/C while in the HDC of TCM the sequence is Pd/C > Pt/C > Rh/C > Ru/C. The activity of the catalysts is related to the electronic properties of the metals and their oxidation states. In the HDC of DCM,

high selectivities to non-chlorinated products were obtained with all the catalysts (>90% in most cases), within the whole range of space–time and reaction temperature investigated. In the HDC of TCM, significantly higher selectivities to DCM were observed with Rh/C and Ru/C. Moreover, these catalysts favored the formation of hydrocarbons larger than methane and the formation of unsaturated hydrocarbons, which can be attributed to a lower metal hydrogenolysis–hydrogenation activity, a higher proportion of electrodeficient species, a lower dispersion of the active phase and a less homogeneous distribution of the active phase on the catalyst. The analysis of the evolution of yields and selectivities to reaction products with space–time suggests that in the HDC of DCM with Pd/C, Pt/C and Rh/C, and in the HDC of TCM with Pd/C and Pt/C, all products are primary products, while in the other cases C_2H_6, C_3H_8, C_4H_{10} and MCM appear to be secondary products formed from the intermediates C_2H_4, C_3H_6, C_4H_8 and DCM. The Pt/C catalyst did not show deactivation after 100 h on stream, while the other catalysts suffered a gradual loss of activity which was much more pronounced in the cases of Rh/C in the HDC of TCM (loss of activity of 75% after 95 h) and Ru/C in the HDC of both DCM (88% after 100 h) and TCM (75% after 58 h).

Acknowledgements

Appendix A. Supplementary data

Supplementary data associated with this article can be found, in the online version, at http://dx.doi.org/10.1016/j.apcatb.2012.11.041.

References

[1] E.D. Goldberg, Science of the Total Environment 100 (1991) 17–28.
[2] W.J. Hayes Jr., E.R. Laws Jr., Handbook of Pesticide Toxicology, Vol. 1: General Principles, Academic Press, San Diego, 1991.
[3] M. Tancrede, R. Wilson, L. Zeise, E.A.C. Crouch, Atmospheric Environment 21 (1987) 2187–2205.
[4] B.H. Carpenter, D.L. Wilson, Journal of Hazardous Materials 17 (1988) 125–148.
[5] F.W. Karasek, R.E. Clement, A.C. Viau, Journal of Chromatography A 239 (1982) 173–180.
[6] B. Coq, G. Ferrat, F. Figueras, Journal of Catalysis 101 (1986) 434–445.
[7] W.J. Makkee, A. Wiersma, E.J.A.X. van de Sandt, H. van Bekkum, J.A. Moulijn, Catalysis Today 55 (2000) 125–137.
[8] A. Wiersma, E.J.A.X. van de Sandt, M.A. den Hollander, H. van Bekkum, M. Makkee, J.A. Moulijn, Journal of Catalysis 177 (1998) 29–39.
[9] M.A. Alvarez-Montero, L.M. Gomez-Sainero, J. Juan-Juan, A. Linares-Solano, J.J. Rodriguez, Chemical Engineering Journal 162 (2010) 599–608.
[10] D. Chakraborty, P.P. Kulkarni, V.I. Kovalchuk, J.L. d'Itri, Catalysis Today 88 (2004) 169–181.
[11] M. Legawiec-Jarzyna, A. Srebowata, W. Juszczyk, Z. Karpinski, Journal of Molecular Catalysis A: Chemical 224 (2004) 171–177.
[12] M. Legawiec-Jarzyna, A. Srebowata, W. Juszczyk, Z. Karpinski, Applied Catalysis A 271 (2004) 61–68.
[13] M. Legawiec-Jarzyna, A. Srebowata, W. Juszczyk, Z. Karpinski, Reaction Kinetics and Catalysis Letters 87 (2006) 291–296.
[14] M.A. Alvarez-Montero, L.M. Gomez-Sainero, M. Martin-Martinez, F. Heras, J.J. Rodriguez, Applied Catalysis B 96 (2010) 148–156.
[15] M.A. Alvarez-Montero, L.M. Gomez-Sainero, A. Mayoral, I. Diaz, R.T. Baker, J.J. Rodriguez, Journal of Catalysis 279 (2011) 389–396.
[16] T. Mori, T. Yasuoka, Y. Morikawa, Catalysis Today 88 (2004) 111–120.
[17] L.M. Gomez-Sainero, A. Cortes, X.L. Seoane, A. Arcoya, Industrial and Engineering Chemistry Research 39 (2000) 2849–2854.
[18] J.L. Benítez, G. del Angel, Industrial and Engineering Chemistry Research 50 (2011) 2678–2682.
[19] V.I. Kovalchuk, J.L. d'Itri, Applied Catalysis A 271 (2004) 13–25.
[20] H. Jüntgen, Fuel 65 (1986) 1436–1446.
[21] R.M. Clark, B.W. Lykins Jr., Granular Activated Carbon: Design, Operation and Cost, Lewis Publishers, Michigan, 1991.
[22] C. Amorim, G. Yuan, P.M. Patterson, M.A. Keane, Journal of Catalysis 234 (2005) 268–281.
[23] C.A. González, M. Bartoszek, A. Martin, C. Montes de Correa, Industrial and Engineering Chemistry Research 48 (2009) 2826–2835.
[24] Z.M. de Pedro, L.M. Gomez-Sainero, E. Gonzalez-Serrano, J.J. Rodriguez, Industrial and Engineering Chemistry Research 45 (2006) 7760–7766.
[25] L. Prati, M. Rossi, Applied Catalysis B 23 (1999) 135–142.
[26] S. Ordonez, H. Sastre, F.V. Diez, Applied Catalysis B 25 (2000) 49–58.
[27] L.M. Gomez-Sainero, X.L. Seoane, J.L.G. Fierro, A. Arcoya, Journal of Catalysis 209 (2002) 279–288.
[28] S.H. Ali, J.G. Goodwin Jr., Journal of Catalysis 176 (1998) 3–13.
[29] N. Mahata, V. Vishwanathan, Catalysis Today 49 (1999) 65–69.
[30] P.P. Kulkarni, S.S. Deshmukh, V.I. Kovalchuk, J.L. d'Itri, Catalysis Letters 61 (1999) 161–166.
[31] S. Somboonthanakij, O. Mekasuwandumrong, J. Panpranot, T. Nimman-wudtipong, R. Strobel, S.E. Pratsinis, P. Praserthdam, Catalysis Letters 119 (2007) 346–352.
[32] J.L. Gasser-Ramirez, B.C. Dunn, D.W. Ramirez, E.P. Fillerup, G.C. Turpin, Y. Shi, R.D. Ernst, R.J. Pugmire, E.M. Eyring, K.A. Pettigrew, D.R. Rolison, J.M. Harris, Journal of Non-Crystalline Solids 354 (2008) 5509–5514.
[33] S. Brunauer, L.S. Deming, W.E. Deming, E. Teller, Journal of the American Chemical Society 62 (1940) 1723–1732.
[34] T. Mori, K. Hirose, T. Kikuchi, J. Kubo, Y. Morikawa, Journal of The Japan Petroleum Institute 45 (2002) 256–259.
[35] P.A. Cox, The Electronic Structure and Chemistry of Solids, Oxford University Press, Oxford, 1987 (Chapter 3, p. 63).
[36] T.T. Phuong, J. Massardier, P. Gallezot, Journal of Catalysis 102 (1986) 456–459.
[37] A. Arcoya, A. Cortes, J.L.G. Fierro, X.L. Seoane, Studies in Surface Science and Catalysis 68 (1991) 557–564.
[38] M. Vaarkamp, J.T. Miller, F.S. Modica, G.S. Lane, D.C. Koningsberger, Studies in Surface Science and Catalysis 75 (1993) 809–820.
[39] G. Larsen, G.L. Haller, Studies in Surface Science and Catalysis 75 (1993) 297–309.
[40] C. Kittel, Introduction to Solid State Physics, Wiley, New York, 1986 (Chapter 6, pp. 139–170).
[41] H.J. Albert, L.R. Rubin, Platinum Group Metals and Compounds, American Chemical Society, Washington DC, 1971 (Chapter 1, pp. 1–16).
[42] F.J. Urbano, J.M. Marinas, Journal of Molecular Catalysis A: Chemical 173 (2001) 329–345.
[43] R. Weast, M. Astle, W. Beyer, CRC Handbook of Chemistry and Physics: A Ready-reference Book of Chemical and Physical Data, CRC Press, Boca Raton, Florida, 1983.
[44] J. Bedia, L.M. Gómez-Sainero, J.M. Grau, M. Busto, M. Martin-Martinez, J.J. Rodriguez, Journal of Catalysis 294 (2012) 207–215.
[45] S. Omar, J. Palomar, L.M. Gómez-Sainero, M.A. Álvarez-Montero, M. Martin-Martinez, J.J. Rodriguez, Journal of Physical Chemistry C 115 (2011) 14180–14192.
[46] L.M. Gómez-Sainero, X.L. Seoane, A. Arcoya, Applied Catalysis B 53 (2004) 101–110.